Fachtagung „Lasermethoden in der Strömungsmesstechnik“
8.-10 September 2015, Dresden

Lagrangian Characterization of Buffet-Induced Flow Separation – A Comparative Analysis of Tomographic-PIV and LES Data

Lagrange’sche Charakterisierung von stoßinduzierten Ablösungen – Ein Vergleich von HS-TPIV und LES Daten

F. Kaiser[1], A. Feldhusen[2], B. Roidl[2], M. Klaas[2] und J. Kriegseis[1]
[1] Institute of Fluid mechanics (ISTM), Karlsruhe Institute of Technology (KIT), Kaiserstraße 10, 76131 Karlsruhe, Germany

[2] Chair of Fluid Mechanics and Institute of Aerodynamics (AIA), RWTH Aachen University, Wüllnerstraße 5a, 52062 Aachen, Germany

Key words: oscillating shock position, Lagrangian flow characterization
Schlagworte: ozillierende Stoßposition, Lagrange’sche Strömungscharakterisierung

Abstract

Lagrangian flow characterization experiences increasing importance in fluid dynamics. Today, its application to experimentally obtained field information is still trailing behind its usage on velocity information acquired by computational fluid dynamics (CFD). This report therefore addresses the attempt to apply a Lagrangian visualization method (Finite-time Lyapunov exponent (FTLE)) on data obtained by highspeed tomographic particle image velocimetry (HS-TPIV) measurements of a transonic flow over an airfoil with oscillating shock position (buffet). For comparison purposes, corresponding large-eddy simulation (LES) results are considered as well. The temporal resolution of the velocity fields appears to be a crucial factor for the transformation of Eulerian to Lagrangian data. Consequently, its influence on the FTLE results is discussed and first steps towards a possible design strategy for future experiments are outlined. Since the FTLE highlights periodic flow features of different frequencies in the buffet flow, a proper orthogonal decomposition (POD) is applied to separate those characteristic flow attributes. The combined usage of the Eulerian POD and the Lagrangian FTLE leads to valuable findings about cause and effects in the flow.

Motivation

Nowadays, the interpretation of flow fields based on Lagrangian methods and visualization techniques is regarded as increasingly important when it comes to the analysis of transport phenomena, mixing processes, recirculation zones, and vortical structures. Examples include the blood flow through the mitral valve of the left ventricle of the human heart (Slotosch et al. 2014), the analysis of cyclic variations in internal combustion engines during the intake and compression stroke, and the flow separation during buffet flow over supercritical wings (Feldhusen et al. 2014), either based on fully three-dimensional time-resolved experimental investigations or on numerical simulations of the flow field.

However, numerical results require validation, e.g., due to the sensitivity of the flow field on the boundary conditions. Moreover, in many cases the numerical simulation of a sufficiently large time interval is not feasible, yet. For instance, the analysis of cyclic variations in internal combustion engines requires the simulation of a minimum number of at least 50 complete engine cycles using LES or direct numerical simulation (DNS) (Granet el al. 2012, Goryntsev et al. 2009), which is not yet economically efficient due to the high computing costs, especially when different engine configurations are to be examined in detail.

Hence, it still is inevitable to perform experimental investigations, e.g., time-resolved volumetric velocity measurement like HS-TPIV with a temporal and spatial resolution that both satisfy the requirements for the application of Lagrangian methods. However, the numerical results can help to design the experiments

especially concerning the temporal resolution in such a way that Lagrangian visualization techniques like the FTLE method can be applied to the experimental findings.

The present work comprises such a design study, which is retroactively performed on the grounds of a direct HS-TPIV/LES comparison. Particularly, either data set will first be processed with both Lagrangian (FLTE) and Eulerian (POD) approaches in order to identify Lagrangian and statistically coherent structures in the respective flow fields. The spatio-temporal character of the extracted patterns is then further analyzed such that a first step towards an interrelation of temporal resolution and uncovered information is outlined.

Considered Velocity Information

The processed velocity fields at hand comprise both HS-TPIV data and LES results of the buffet flow around a DRA 2303 profile under cruise-flight conditions. While the flow conditions of the different data sets are comparable, both temporal and spatial resolution differ substantially between PIV and LES data. Table 1 provides an overview of the characteristics of the data sets. To ensure comparability, the dimensionless LES results are converted into the experimental configuration. Further, for the applicability of the FTLE-tool in hand, the LES velocity data has been interpolated on a fine equidistant grid.

data set	**HS-TPIV**	**LES**
angle of attack α	3.5°	3°
chord length c	150 mm	150 mm
$Re_c = u_\infty c/\nu$	$2 \cdot 10^6$	$2.6 \cdot 10^6$
M_∞	0.73	0.73
observed area	trailing edge region (see Figure 1)	far field extension $25c$
data points	22134 $(61 \cdot 52 \cdot 7)$	$\approx 30 \cdot 10^6$ (before interpolation)
sample rate	$f_{PIV} = 1000$ Hz	$f_{LES} \approx 165000$ Hz
buffet frequency f_b	$\approx$ 170 Hz	$\approx$ 170 Hz
velocity fields per buffet cycle	$\approx$ 6	$\approx$ 970
number of captured buffet cycles	$\approx$ 340	$\approx$ 3
data points/c	$\approx$ 126	1000

Table 1: Comparison of the velocity data from HS-TPIV measurements and LES simulations

It should be noted, that two different coordinate systems are used in this report. The HS-TPIV data is provided in a coordinate system aligned to the upper surface of the profiles hind part (see Figure 1), whereas the x-axis of the LES coordinate system is parallel to the chord. A brief review of the acquisitions of the data sets is given below.

Tomographic Particle-Image Velocimetry

Tomographic Particle-Image Velocimetry has been applied to analyse the buffet flow field in a measurement volume located in the trailing-edge region of the airfoil. The experiments have been performed in the Trisonic wind tunnel of the Institute of Aerodynamics RWTH Aachen University, which is an intermittent working vacuum storage tunnel with an adaptive test section whose cross section measures 40 cm x 40 cm. The two-dimensional supercritical laminar-type DRA 2303 airfoil model is made of an orthotropic ultra-high modulus carbon fiber laminate sandwich shell. Transition is fixed at $0.05c$ by a 117 µm zigzag

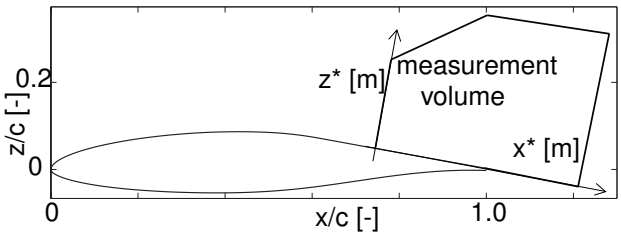

Figure 1: Measurement volume and coordinate system of the HS-TPIV-setup

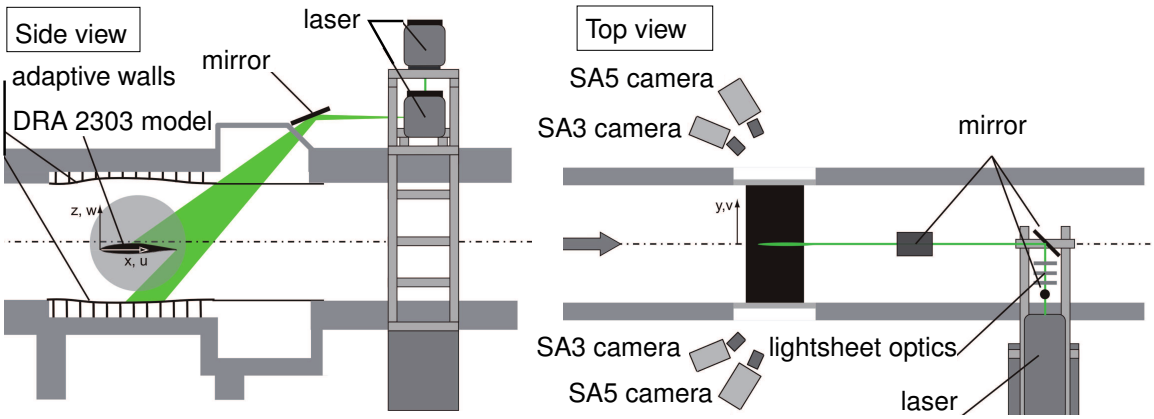

Figure 2: HS-TPIV-setup at the Trisonic wind tunnel

shaped transition strip.The tomographic PIV setup is shown in Figure 2. DEHS oil droplets were used as seeding particles. The illumination of the volume was performed with 2 high-speed double-pulsed Nd:YLF lasers emitting light with a wave length of 527 nm, the laser sheet thickness was 6 mm. The acquisition of the images was done by four Photron Fastcams equipped with 180 mm Tamron lenses. The resulting frequency was 1000 Hz. The evaluation of the raw images was done with DaVis by LaVision, applying a volumetric self calibration, reconstructing the volume by a fastMART algorithm and correlating with a multi-pass interrogation method. A detailed description of the experiments can be found in Feldhusen et al. 2014.

Large eddy simulation

The Navier-Stokes equations for three-dimensional unsteady compressible flow are discretized by a mixed centered upwind AUSM (advective upstream splitting method) scheme at second-order accuracy for the Euler terms and the non-Euler terms are discretized second-order accurate using a centered approximation. The temporal integration is done by a second-order explicit 5-stage Runge-Kutta method. A detailed description of the fundamental LES solver is given in Meinke et al. 2002. The transition is fixed at the pressure and suction side of the airfoil at $x/c = 0.05$ for both numerical configurations by introducing a wall surface roughness of an amplitude of approximately 10 inner wall units or $8 \cdot 10^{-4} \Delta y/c$. The resolution of the pure LES grid in the streamwise, the wall-normal, and the spanwise direction is $\Delta x^+ \approx 50$, $\Delta y^+_{min} \approx 1$, and $\Delta z^+ \approx 2$, yielding $30 \cdot 10^6$ grid points. The resulting time step does not exceed $2 \cdot 10^-6 c/u_\infty$. The C-grid has a far-field extension of $25c$ and a spanwise extension of $0.021c$. Non-reflecting boundary conditions are set at the far field boundaries, periodic boundary conditions in the spanwise direction, and adiabatic wall-boundary conditions at the airfoil surface. A similar flow configuration was also investigated in Roidl et al. 2011. Note that the sampling time step of the flow solutions was set to 0.01 c/u_∞ which is about 6 µm based on the experimental flow configuration.

Applied Processing Approaches

The Finite Time Lyapunov Exponent

Due to their great potential in visualizing flows, Lagrangian coherent structures (LCS) have gained importance in current research. In two dimensional flows LCS are material lines separating areas of coherent movement. Thereby, not only vortex boundaries and recirculation zones are detected but also other flow structures are outlined, if their movement differs from the movement of the fluid around them.

A distinction must be made between two different types of LCS. Repelling LCS (indicated blue throughout the report) push neighboured particles aside while attracting LCS (indicated red accordingly) keep on pulling them towards the manifold. Besides the obvious feature of being material separatrices, the mentioned repelling or attracting properties of LCS provide additional information about the flow around the identified structures.

The FTLE evaluates local stretching in between neighboured particles and thereby allows to determine

LCS. A short introduction into the determination of the FTLE is given in the following section. For more detailed information please refer to Slotosch et al. 2014 and Shadden et al. 2005.

Starting with unsteady Eulerian data a fine grid of massless particles is virtually seeded in the flow. During an integration time T_{int} the particles are tracked by solving the ordinary differential equation $\dot{x}(x_0,t) = u(x(x_0,t),t)$. The resulting flow map $\Phi_{t_0}^{t_0+T_{int}}$ describes the perturbation of a particle during the integration time and is used to determine the right Cauchy-Green deformation tensor

$$C = (\nabla\Phi_{t_0}^{t_0+T_{int}})^{\mathrm{T}}\nabla\Phi_{t_0}^{t_0+T_{int}} \quad .$$

As the positive definite matrix C provides the local stretching during the integration time, the maximum eigenvalue $\lambda_{max}(C)$ allows to determine its maximum. Finally, some normalizations are applied and lead to the FTLE

$$\sigma_{t_0}^{t_0+T_{int}} = \frac{1}{|T_{int}|}\ln\sqrt{\lambda_{max}(C)} \quad .$$

The ridges of the FTLE field are defined as hyperbolic LCS. Ordinary integration of the velocity data forward in time (forward FTLE) leads to the identification of repelling LCS. However, if particles are tracked backward in time (backward FTLE), the FTLE can also be used to determine attracting LCS.

Proper orthogonal decomposition

To extract Eulerian statistically coherent structures of potentially harmonic character from the flow field, the data is further decomposed by means of POD. A brief introduction into POD is provided below, adapted from Kriegseis et al. 2010 and Mattern et al. 2015.

First, an unsteady velocity information can be separated into its average and its instantaneous deviation from this average by means of the Reynolds decomposition $\tilde{u}(x,t^i) = \bar{u}(x) + u(x,t^i)$, where $i \in N$ indicates the respective velocity fields of the basis N. In general, a POD separates spatially correlated but temporally inhomogeneous flow structures from uncorrelated random fluctuations (noise), both of which are contained in the deviations $u(x,t^i)$ (i.e. the rms-field). These deviations u^i can be arranged to form a covariance matrix $R = UU^T$, where $U = [u^1, u^2 \ldots u^N]$. The solution of the eigenvalue problem

$$R\Phi = \lambda\Phi$$

leads to the POD Modes ϕ_j (eigenvectors) with corresponding eigenvalues λ_j. The resulting contribution of each Mode j to the overall signal power is given by $P_j = \lambda_j/||\lambda||$. If the eigenvalues are ordered decreasingly, the first few Modes ϕ_j of the matrix $\Phi = [\phi_1, \phi_2, \ldots, \phi_N]^T$ contain the main part of the energy in the recorded flow scenario. The impact of each Mode ϕ_j to the individual snap shots u^i can be determined in terms of the weighting coefficients $a_j^i = \phi_j u^i$. Note that the average $\bar{a}_j$ of a_j^i over N snapshots is zero by definition, i.e. $\bar{a}_j = 1/N\Sigma_{i=1}^{N} a_j^i \stackrel{!}{=} 0$. In case of time-resolved velocity information, the histories of extracted coefficients $a_j^i = a_j(t^i)$ additionally provide insight into the temporal thus harmonic behavior of the respective modes. As such, the frequency information in the flow can be immediately linked to the corresponding flow patterns.

Results and Discussion

Lagrangian Approach - FTLE Results

In this section the applicability of the FTLE on the measured HS-TPIV data is discussed and compared to FTLE fields of the LES data. For both data sets the integration time for the FTLE was chosen as $|T_{int}| = 1/3 \cdot c/u_\infty = \ 2 \cdot 10^{-4}$s to ensure sufficient particle displacement, which in turn implies that a particle travel of approx. 33% chord c during the integration time in the outer free stream.

However, to measure a large field of view on the suction side of the wing, the experiment had to be chosen in such a way, that all cameras still operate at full spatial resolution. This means that all four cameras recorded the flow with a frequency of 2000 Hz (corresponding to a sample rate of 1000 Hz)

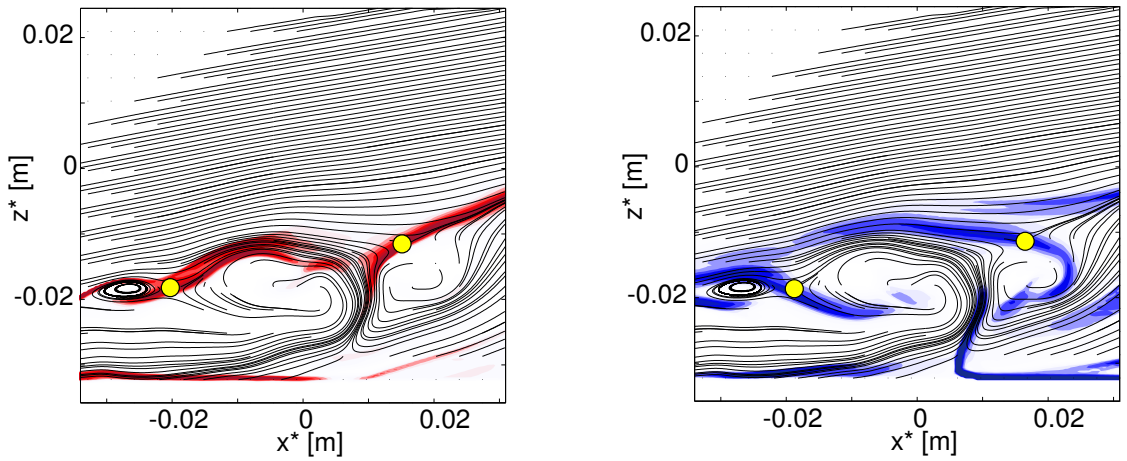

Figure 3: HS-TPIV data: Streamlines compared to the FTLE field: Attracting (red) and repelling (blue) ridges; saddles (yellow).

and a spatial resolution of 1024×1024 px^2. Hence, the transformation of the information into Lagrangian properties is hardly possible, since the particles cross the measurement volume almost twice per time step $T_{PIV} = 10^{-3}$s. As a result, the calculated particle paths are based on quasi stationary velocity data. In this particular case with $|T_{int}| \ll T_{PIV}$, the FTLE ridges indicate the separatrices of streamlines rather than path-line related information (see Figure 3) and the intersection of forward and backward FTLE defines saddle points of the Eulerian field.

To investigate the influence of the temporal resolution on the FTLE from the LES data, the time step is artificially increased from the original time step $T_{LES} = 6 \cdot 10^{-6}$s to $T_{LES}^{165} = 165 \cdot T_{LES} \approx T_{PIV}$. The results of the subsequent FTLE calculation for either temporal resolution is shown in Figure 4. Here, it is particularly important to be aware of the transition from pathline-based to quasi streamline-based visualization of the ridges, to avoid a physical misinterpretation of the flow field. Nonetheless, the direct comparison of

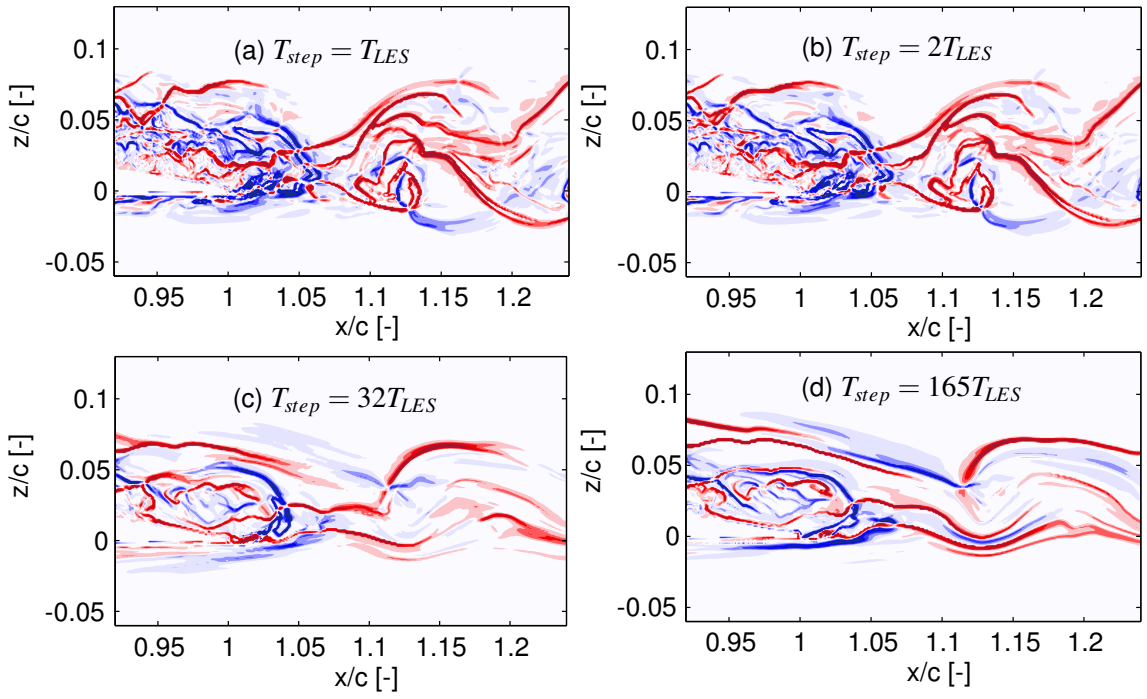

Figure 4: LES data: Development of the FTLE results at the trailing-edge with decreasing temporal resolution of the velocity data

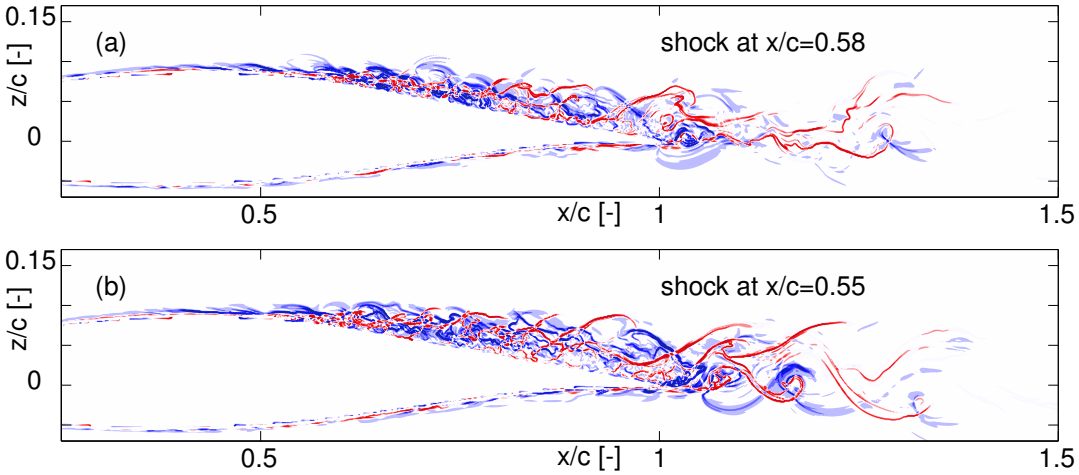

Figure 5: Repelling (blue) and attracting (red) LCS of the LES data; (a) small separation, fast boundary layer; (b) large separation, slow boundary layer

Figures 4(a) and (b) demonstrates sufficient temporal resolution of the original LES data, as the shape of the extracted LCS ridges does not change here.

As shown in Figure 5 the buffet-induced flow oscillation becomes obvious from the flow-field comparison between the two most separated shock positions. Figure 5(a) reveals a more attached flow while the shock is placed downstream. Correspondingly, Figure 5(b) shows a larger separated region as the shock is positioned upstream. Further evaluation of consecutive FTLE fields (not shown here for brevity) uncovers that in addition to the dimensions of the separated region also the flow magnitude within this zone varies significantly with shock-position changes. Particularly, in case of the most upstream located shock, the flow in the separated zone is near zero and/or partly reversed.

Moreover, the comparison of Figures 5(a) and (b) indicates the correlation between separation-zone size and coherence, strength and dimensions of the shed vortical structures. Note, however, that only the separation-zone size and shock position oscillate at identical frequency. The trailing-edge vortices, in contrast, shed at a much higher frequency and only the intensity of the structures changes with the buffet frequency.

Eulerian Approach - POD Analysis

Complementary to the above FTLE analysis, the oscillatory character of the buffet-induced flow-field fluctuations directly suggests an investigation into statistically coherent patterns (Modes) superimposed onto the average flow field by means of POD. As outlined above, the flow scenario at hand is primarily comprised of two such harmonic flow patterns, i.e., the oscillating separation zone and the vortex shedding into the wake.

Figure 6 clearly demonstrates that the most powerful ($P_1 = 0.39$) flow pattern of the HS-TPIV data covers

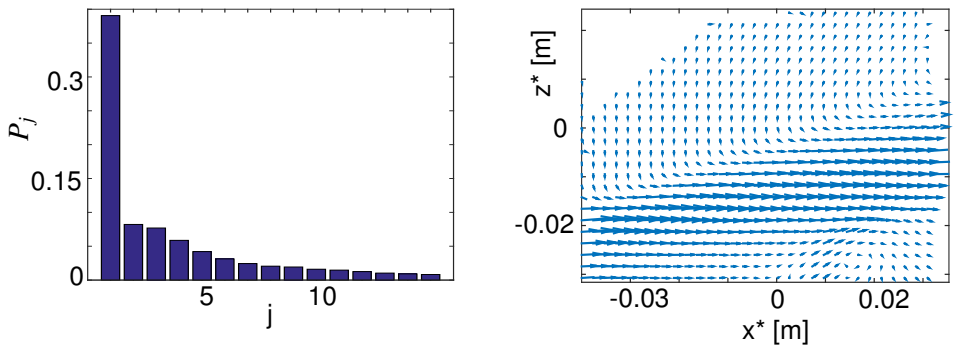

Figure 6: HS-TPIV data: Power P_j of the POD Eigenvalues (left) and first Mode ϕ_1 (right)

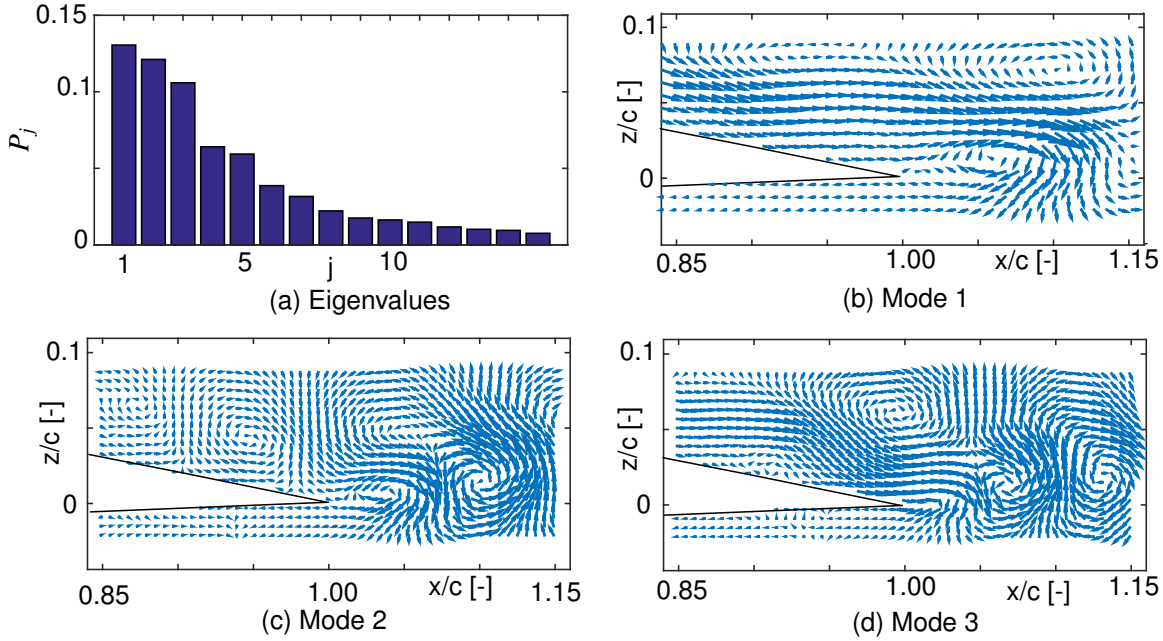

Figure 7: LES data: Power P_j of the POD Eigenvalues and Modes 1-3

the coherent dynamics of the separated region. However, the frequency content of the reconstructed coefficient $a_1^{PIV}(t)$ does not contain a distinct peak even though the HS-TPIV sample rate is well above the Nyquist criterion of the buffet oscillation ($f_{PIV} \approx 6 f_b$).

To investigate this seeming discrepancy more rigorously, the POD results of the LES data is considered as well (see Figure 7). Similar to the HS-TPIV results, the pattern of LES-Mode 1 (Figure 7b) corresponds to the oscillatory separation. Furthermore, the history of the reconstructed coefficient $a_1^{LES}(t)$ indicates the periodicity of the buffet oscillation as plotted in Figure 8(a). Moreover, both a strong cycle-to-cycle variation (sweep and shape) as well as high amounts of higher frequencies can be identified from the diagram. This insight retroactively explains the results of the a_1^{PIV}-analysis.

Furthermore, Modes 2 and 3 represent the shedding vortices. As their coefficients have a distinct phase relation (Figure 8b) and the flow patterns of Modes 2 and 3 are displaced accordingly (Figure 7c+d), the superposition of Mode 2 and 3 leads to propagating vortices. Note that two time periods are shaded in Figures 8(a) and (b), which represent the cases of strong (blue) and mild (grey) flow separation,

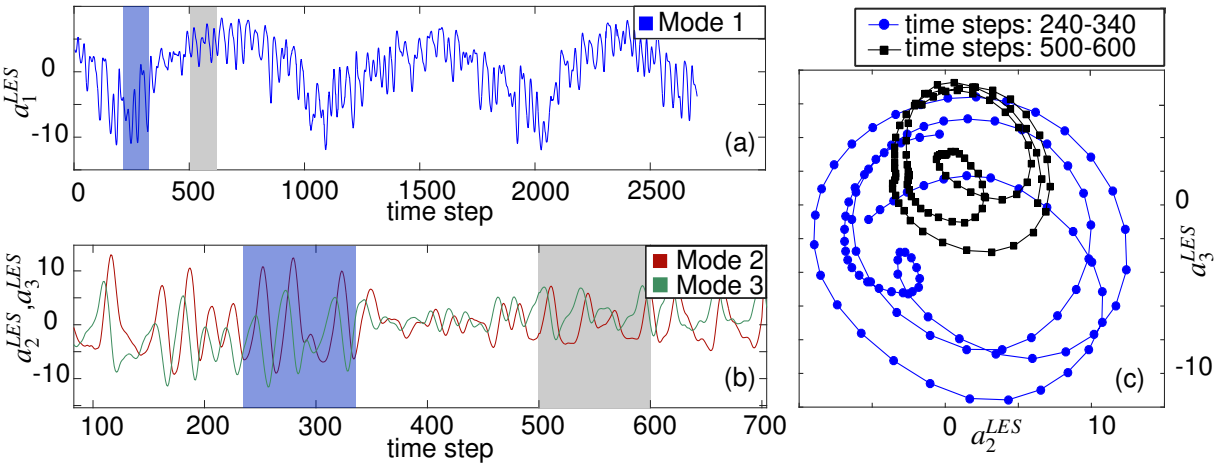

Figure 8: LES data: Histories of the reconstructed coefficients $a_j^{LES}(t)$: (a) Mode 1, (b) Modes 2 and 3, (c) Lissajous figure of a_2^{LES} and a_3^{LES} for negative (●) and positive (■) values of a_1^{LES}

respectively. Comparing the coefficients of Mode 2 and 3 during those time spans 8(c) demonstrates that the pair of modes is largely dominated by a 90° phase relation with separation-dependent magnitude. This dependency immediately supports the qualitative observation made by the FTLE, which indicates the necessity to analyse the relationship between shock position and vortex strength.

Concluding Remarks

The performed comparison of HS-TPIV and LES data, both describing the phenomenon of buffet flow separation, displayed the challenges of transferring Eulerian fields to Lagrangian informations. Particularly, in high Reynolds number flows it is essential to capture velocity data of sufficient spatial and temporal resolution. The application of Lagrangian approaches to experimental data, which were acquired with sampling frequencies that were chosen to extract Eulerian information, might lead to misinterpretations concerning the topology of the flow. In order to apply Lagrangian methods on experimental results, the experimental set-up has to be designed in regard to the necessities of this transformation process. The minimum required temporal (and spatial) resolution of a experiment is definable by systematically cropping CFD data of a comparable problem and evaluating the results of FTLE calculations. In continuation of current investigations by Slotosch et al. 2015, upcoming efforts will elaborate such an evaluation strategy, which varies the temporal and spatial resolution on basis of CFD data, determines the deviation of LCS positions and thereby predicts the error of a potential experimental set-up. In addition to the insights into the requirements of data acquisition, the FTLE provided a qualitative overview concerning the buffet flow characteristics and lead to the application of the POD, which identified the oscillating separation in both data sets. The POD results of the LES data helped to understand the limited access to a distinct buffet frequency presumingly contained in the HS-TPIV data and uncovered the dependency of the trailing-edge vortex strength on the buffet position.

References

[1] A. Feldhusen, A. Hartmann, M. Klaas, and W. Schröder. High-speed tomographic piv measurements of buffet flow over a supercritical airfoil. In *17th Int. Symp. on Appl. of Laser Techniques to Fluid Mechanics, Lisbon, Portugal, 2014.*, 2014.

[2] D. Goryntsev, A. Sadiki, M. Klein, and J. Janicka. Large eddy simulation based analysis of the effects of cycle-to-cycle variations on air–fuel mixing in realistic disi ic-engines. *Proceedings of the Combustion Institute*, 32(2):2759–2766, 2009.

[3] V. Granet, O. Vermorel, C. Lacour, B. Enaux, V. Dugué, and T. Poinsot. Large-eddy simulation and experimental study of cycle-to-cycle variations of stable and unstable operating points in a spark ignition engine. *Combustion and Flame*, 159(4):1562–1575, 2012.

[4] J. Kriegseis, T. Dehler, M. Gnirß, and C. Tropea. Common-Base Proper Orthogonal Decomposition (CPOD) as a Means of Quantitative Data Comparison. *Meas. Sci. Technol.*, 21:085403, 2010.

[5] P. Mattern, J. Kriegseis, and M. Gabi. Flow Characteristics beyond Time and Phase - A Modal Analysis of the Patterns in a Regenerative Pump. In *International Conference on Fan Noise, Technology and Numerical Methods - FAN2015, Lyon, France*, 2015.

[6] M. Meinke, W. Schröder, E. Krause, and Th. Rister. A comparison of second- and sixth-order methods for large-eddy simulations. *Computers & Fluids*, 31:695–718, 2002.

[7] B. Roidl, M. Meinke, and W. Schröder. Zonal rans-les computation of transonic airfoil flow. *AIAA Paper, AIAA*, pages 2011–3974, 2011.

[8] S.C. Shadden, F. Lekien, and J.E. Marsden. Definition and properties of lagrangian coherent structures from finite-time lyapunov exponents in two-dimensional aperiodic flows. *Physica D: Nonlinear Phenomena*, 212(3): 271–304, 2005.

[9] A. Slotosch, J. Schlanderer, F. Kaiser, and J. Kriegseis. Heart flow vortices – an application of flow characterization techniques. In *22. Fachtagung Lasermethoden in der Strömungsmesstechnik, Karlsruhe, Germany*, 2014.

[10] A. Slotosch, M. Gollub, F. Kaiser, B. Frohnapfel, and J. Kriegseis. Lagrangian coherent structures in unsteady flow fields – required resolution of the field information. In *23. Fachtagung Lasermethoden in der Strömungsmesstechnik, Dresden, Germany*, 2015.